analytical chemistry

Article

pubs.acs.org/ac

Real-Time Analysis of Cellular Response to Small-Molecule Drugs within a Microfluidic Dielectrophoresis Device

In Soo Park,[†] Jaewoo Lee,[†] Gyudo Lee,[†,∥] Kihwan Nam,[†] Taewoo Lee,[†] Woo-Jin Chang,[‡] Hansung Kim,[†] Sei-Young Lee,[†] Jongbum Seo,[†] Dae Sung Yoon,[§] and Sang Woo Lee*[,†]

[†]Department of Biomedical Engineering, Yonsei University, Wonju 220-710, Republic of Korea

[‡]Department of Mechanical Engineering and Great Lakes WATER Institute, University of Wisconsin−Milwaukee, Milwaukee, Wisconsin 53211, United States

[§]School of Biomedical Engineering, Korea University, Seoul, 136-703, Republic of Korea

[∥]T.H. Chan School of Public Health, Harvard University, Boston, Massachusetts 02115, United States

Supporting Information

ABSTRACT: Quantitative detection of the biological properties of living cells is essential for a wide range of purposes, from the understanding of cellular characteristics to the development of novel drugs in nanomedicine. Here, we demonstrate that analysis of cell biological properties within a microfluidic dielectrophoresis device enables quantitative detection of cellular biological properties and simultaneously allows large-scale measurement in a noise-robust and probeless manner. Applying this technique, the static and dynamic biological responses of live B16F10 melanoma cells to the small-molecule drugs such as *N*-ethylmaleimide (NEM) and [(dihydronindenyl)oxy]alkanoic acid (DIOA) were quantitatively and statistically examined by investigating changes in movement of the cells. Measurement was achieved using subtle variations in dielectrophoresis (DEP) properties of the cells, which were attributed to activation or deactivation of K^+/Cl^- cotransporter channels on the cell membrane by the small-molecule drugs, in a microfluidic device. On the basis of quantitative analysis data, we also provide the first report of the shift of the complex permittivity of a cell induced by the small-molecule drugs. In addition, we demonstrate interesting quantifiable parameters including the drug effectiveness coefficient, antagonistic interaction coefficient, kinetic rate, and full width at half-maximum, which corresponded to changes in biological properties of B16F10 cells over time when NEM and DIOA were introduced alone or in combination. Those demonstrated parameters represent very useful tools for evaluating the effect of small-molecule drugs on the biological properties of cells.

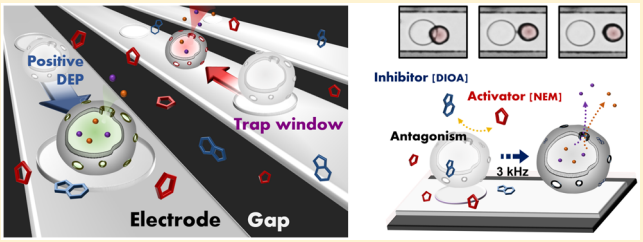

Quantitative characterization of the biological properties of live cells is very important, not only for understanding cellular metabolism, but also for deciphering molecular interactions in cell signaling. Recently, a number of exceptional achievements in this field have been reported. For example, atomic force microscopy (AFM) enables direct measurement of the stiffness of live cells for cancer diagnosis[1] and evaluation of drug effects on cytoskeletal changes.[2] Nanoengineered surfaces (e.g., vertical nanowires and nanostructured electrodes) have been developed to capture circulating tumor cells,[3] detect cellular responses to electrical stimuli,[4] and record intracellular action potentials in the presence of drugs by analyzing cellular dynamics.[5−8] Those approaches are very precise and accurate for quantitatively characterizing cellular biological properties in general. However, these methods only measure single cells or a few cells at a time (e.g., AFM[1,2] and flexible cantilever[6]) or require complicated calibration processes to improve the signal-to-noise ratio (e.g., electrodes[4,5] and biotransistors[7,8]). Additionally, these techniques can distort the original cellular biological properties as a result of injection with, or contact with, a probe. Moreover, it is difficult to conceptualize the properties of nonadherent live cells in three dimensions (3D). In this respect, microfluidic dielectrophoresis (μF-DEP) serves as a simpler and less invasive measurement technique (i.e., a label-free and probeless manipulator) that can remotely control the motion of live cells in a nonuniform electric field induced by different amplitude and frequency of alternating current and different physical conditions, such as conductivity and permittivity between a cell and its surroundings.[9,10] Microfluidic dielectrophoresis devices can also be a powerful platform for studying 3D property changes in live cells, such as cellular responses to small-molecule drugs.[11,12] These devices are useful in cell sorting and manipulation as a result of subtle changes in dielectrophoretic (DEP) properties depending on cell type,[12] size,[13] and surrounding conditions.[14] Moreover, our recent studies have shown that a μF-DEP device can precisely control

Received: November 7, 2014
Accepted: March 15, 2015
Published: March 26, 2015

DOI: 10.1021/ac5041549
Anal. Chem. 2015, 87, 5914−5920

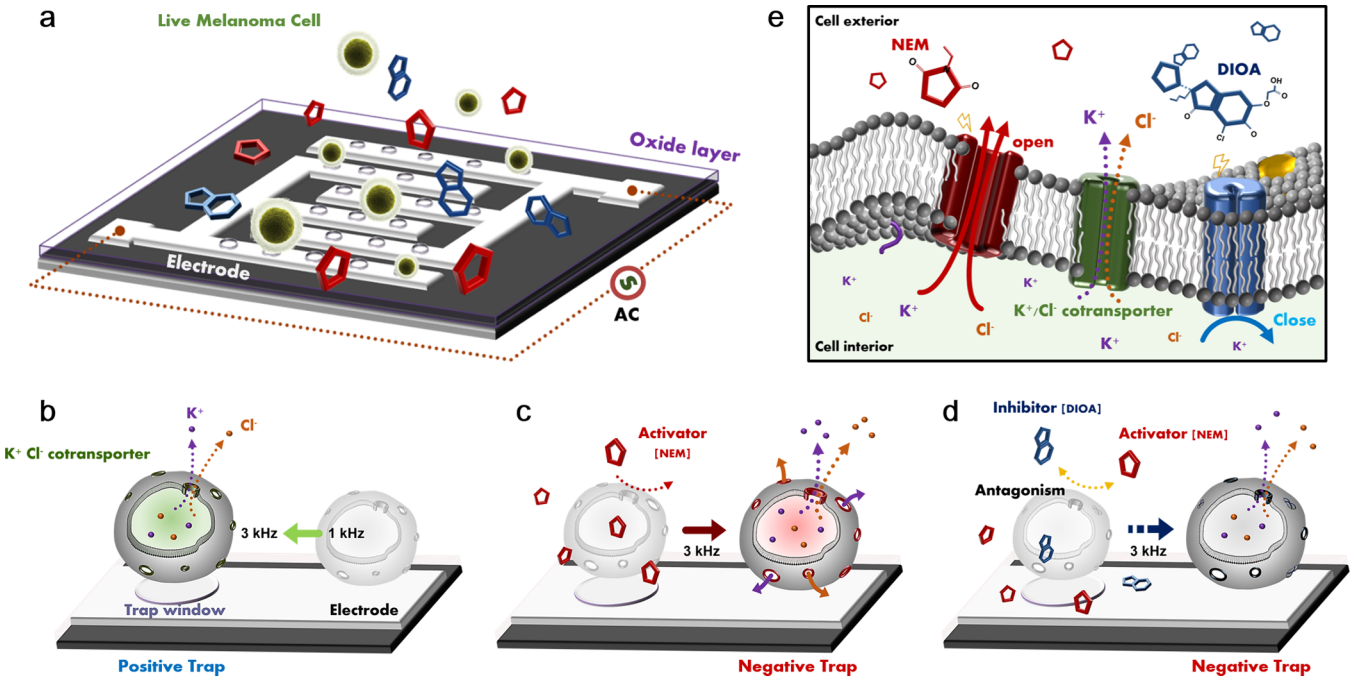

Figure 1. Cellular responses of live cells to small-molecule drugs. (a) Schematic view of fabricated μF-DEP-on-chip with trap windows, in which nonadherent cells were either trapped or released around the window as a result of changes in dielectrophoretic properties of the cells arising from drug−cell interactions. (b−d) Static and dynamic dielectric response of live B16F10 melanoma cells to the small-molecule drugs. (e) Overview of the effects of small-molecule drugs (NEM and DIOA) on the function of K^+/Cl^- cotransporter (KCC) channels distributed on the cell membrane. NEM and DIOA directly bind to KCC channels resulting in channel activation and deactivation, respectively. These drug−cell interactions cause minute variations in the polarizability of the cells, and the resultant cell movements were defined as described in panels b−d.

the dynamics of microparticles, thus allowing quantification of the chemical/physical interactions between chemical functional groups or biomolecules at the single-molecule level.[15−17] This principle can be extended to the quantitative characterization of cellular biological properties in a simple, noninvasive, and noise-robust manner.

Here, we use a μF-DEP device that can measure cellular behavior of at least 200 cells/mm^2 under a microscope in a probeless manner (Figure 1a) to demonstrate a real-time quantitative and statistical analysis technique to measure changes in biological properties of live cells in response to a small-molecule drug or a combination of small-molecule drugs. In this study, live B16F10 melanoma cells served as a nonadherent prototype cell for the study of cellular biological properties because these cells are well-known for their wide applicability in physiology, pharmacology, and the cosmetic industry.[18,19] *N*-Ethylmalemide (NEM) and [(dihydroindenyl)-oxy]alkanoic acid (DIOA) were used as small-molecule drugs; NEM, a sulfhydryl reagent, was used to activate K^+/Cl^- cotransporter (KCC) channels in the cell membrane so that ions would be released from the cell interior, whereas DIOA causes deactivation of these channels.[20,21] This activation or deactivation causes variation in the complex permittivity within the cell, resulting in alterations in DEP behavior of the cell. Furthermore, the combinations of different small-molecule drugs on a cell generate the antagonistic effect, which means the reduction of drug efficiency by independent competition between agonist and antagonist. In this way, cells affected by NEM or DIOA can be trapped or released around trap windows when a DEP force is applied (Figure 1b−d). In our μF-DEP device, the individual DEP behaviors of multiple cells (200 cells/mm^2) were simultaneously observed in real time with various concentrations of NEM and DIOA administered individually and concurrently. Through these observations, the static and dynamic biological responses of the cells were quantitatively and statistically analyzed. These data provide the first report of the shift in cell complex permittivity induced by these small-molecule drugs. Furthermore, we demonstrated several interesting parameters, including full width at half-maximum (fwhm), kinetic rate, drug effectiveness coefficient, and antagonistic interaction coefficient, that can evaluate how the small-molecule drugs affect the cells with regard to static and dynamic responses. Such studies can be used to provide useful information on cellular static and dynamic responses to drugs and drug−drug interplay at the single-cell level.

MATERIALS AND METHODS

Chip Fabrication. To fabricate the microfluidic device, a pattern producing electrode lines that were 30 μm wide and 10 μm apart was formed on an oxide/silicon wafer substrate (i-Nexus, 4-in., wet type) through photolithography. After deposition of a 0.1 μm thick chromium layer on the pattern using a thermal evaporator, a lift-off process was performed. The electrodes were covered with a 0.8 μm SiO_2 layer for insulation using the plasma-enhanced chemical vapor deposition (PECVD) technique. In the final step of this fabrication, circular trap windows were defined on the SiO_2 layer by photolithography. Subsequently, the trap windows were etched resulting in exposure of circular regions on the electrode. A schematic diagram of the device fabrication process flow is shown in Supporting Information Figure S4, and optical images of the electrodes and trap windows are shown in Supporting Information Figure S1c.

Cell Culture. The B16F10 mouse melanoma cell line was obtained from the Korean Cell Line Bank. Cells were cultured

DOI: 10.1021/ac5041549
Anal. Chem. 2015, 87, 5914−5920

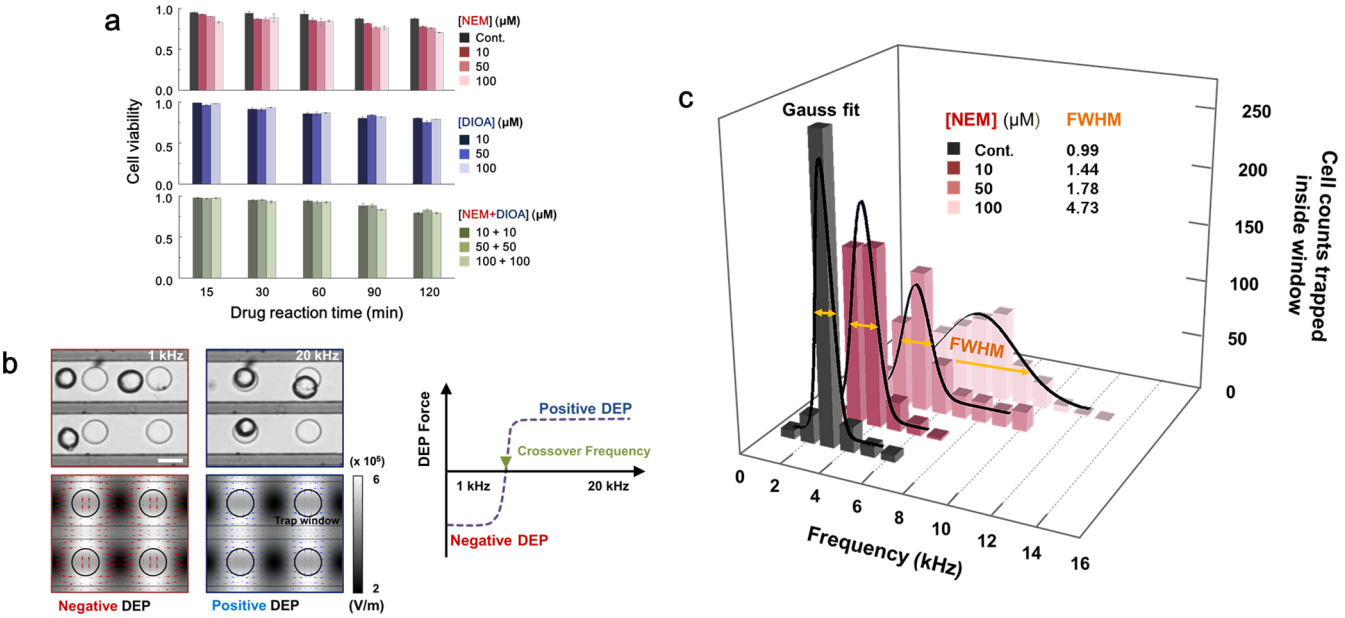

Figure 2. Static cellular responses of live cells to small-molecule drugs. (a) Cell viability test of B16F10 cells exposed to small-molecule drugs (control, NEM, DIOA, and NEM + DIOA; 10−100 μM) for 120 min. (b) Upper panels: optical images of DEP manipulation of live cells with negative and positive DEP show trapping of the cells around the trap windows and the gap between the trap windows when applying a 3 $V_{p\text{-}p}$ at frequencies of 1 and 20 kHz, respectively. Experiments were performed at room temperature in a buffer. The scale bar indicates 20 μm. Lower panels: finite element analysis-based calculations of electric field intensity and DEP force vectors at 10 μm height from the electrode in the microfluidic chip at the same scale as the experimental study were plotted and compared with the experimental results. (c) Number of cells trapped in a trap window vs applied ac voltage at different frequencies (0−15 kHz) at a frequency sweeping rate of 1/30 kHz·s^{-1} and optical images at each chosen frequency for a total of 15 frames. The data in each set were collected 90 min after NEM was added to the medium. The black line shows the fitted Gaussian distribution function of the NEM-treated cells with different NEM concentrations.

in an incubator (5% CO_2, 37.5 °C) with Dulbecco's modified Eagle's medium (DMEM, Lonza) containing 10% fetal bovine serum (FBS), 1% L-glutamine, and 1% penicillin−streptomycin.[28] For experiments the cells were detached by trypsin/EDTA and washed three times before addition to the buffer at a concentration of 10 cells/μL. The experimental buffer consisted of 8.6% (w/w) sucrose, 0.3% (w/w) glucose, and 1.0 mg/mL bovine serum albumin (BSA, Sigma-Aldrich).[28]

Cell Viability Test. Viability of the B16F10 mouse melanoma cells was investigated using Trypan blue (Sigma, T8154) staining. B16F10 cells in the buffer solution were exposed to small-molecule drugs (control, NEM, DIOA, and NEM + DIOA, 10−100 μM) for 0−120 min. After exposure, the solution was mixed with 0.4% Trypan blue solution at a 1:1 ratio and the number of viable cells was counted using a hemocytometer (Marienfeld GmbH, Germany) equipped with an inverted microscope (Bestscope, BS2090).

Experimental Procedures. After placing the poly(dimethylsiloxane) (PDMS) reservoir on the chip, 30 μL of experimental buffer including cells with and without small-molecule drugs (NEM, DIOA, or NEM + DIOA [10−100 μM]) was dropped into the reservoir and a glass cover was placed on top to flatten the buffer droplet. Subsequently, an ac signal was applied to the electrode of the chip at varying amplitudes and frequencies using a function generator (Agilent, 33250A). Cell movement was observed and recorded using a charge-coupled device camera (Artray Co., ARTCAM-150P-DS).

Dielectrophoretic Model Explaining the Behavior of the Cells. In the first approximation, the DEP formula used was as below:[22,29]

$$F_{DEP} = 2\pi\varepsilon_m a^3 \mathrm{Re}[K(\omega)]\nabla|E_{RMS}|^2 \quad (1)$$

where ε_m is the medium permittivity, a is the radius of a particle, $|E_{RMS}|^2$ is the square of the RMS electric field, and $K(\omega)$, called the CM factor, is given by $K(\omega) = (\varepsilon^*_{cell} - \varepsilon^*_m)/(\varepsilon^*_{cell} + 2\varepsilon^*_m)$. ε^*_{cell} and ε^*_m are the complex permittivities of the cell and the medium, in which $\varepsilon^* = \varepsilon + j(\sigma/\omega)$ where ε, σ, and ω are the relative permittivity, conductivity, and frequency, respectively.[29] Assuming that the structure of the cell is the "single-shell" model shown in Supporting Information Figure S1, the complex permittivity of the cells is given as[22,29]

$$\varepsilon^*_{cell} = \varepsilon^*_{mem}\frac{[\lambda^3 + \{(\varepsilon^*_{cyt} - \varepsilon^*_{mem})/(\varepsilon^*_{cyt} + \varepsilon^*_{mem})\}]}{[\lambda^3 - \{(\varepsilon^*_{cyt} - \varepsilon^*_{mem})/(\varepsilon^*_{cyt} + \varepsilon^*_{mem})\}]} \quad (2)$$

where λ is the scaling of cells described as $\lambda = a/(a - t)$, t is the thickness of the cell membrane, and ε^*_{cyt} and ε^*_{mem} are the complex permittivities of the cytoplasm and the cell membrane, respectively. Here we note that the NEM-treated cell can also be assumed to follow the single-shell model because the cells functioned normally despite cellular blebs.[30] On the basis of the above model, numerical analysis was performed. A more detailed explanation is provided in Supporting Information Note 1.

RESULTS

Static Responses Caused by Variation in NEM Concentration. The viability of mammalian B16F10 cells was examined to assess the toxic effects of NEM and DIOA. As shown in Figure 2a, overall cell viabilities under the experimental conditions were more than 70%. Thus, no significant effect of NEM or DIOA on cell viability was

DOI: 10.1021/ac5041549
Anal. Chem. 2015, 87, 5914−5920

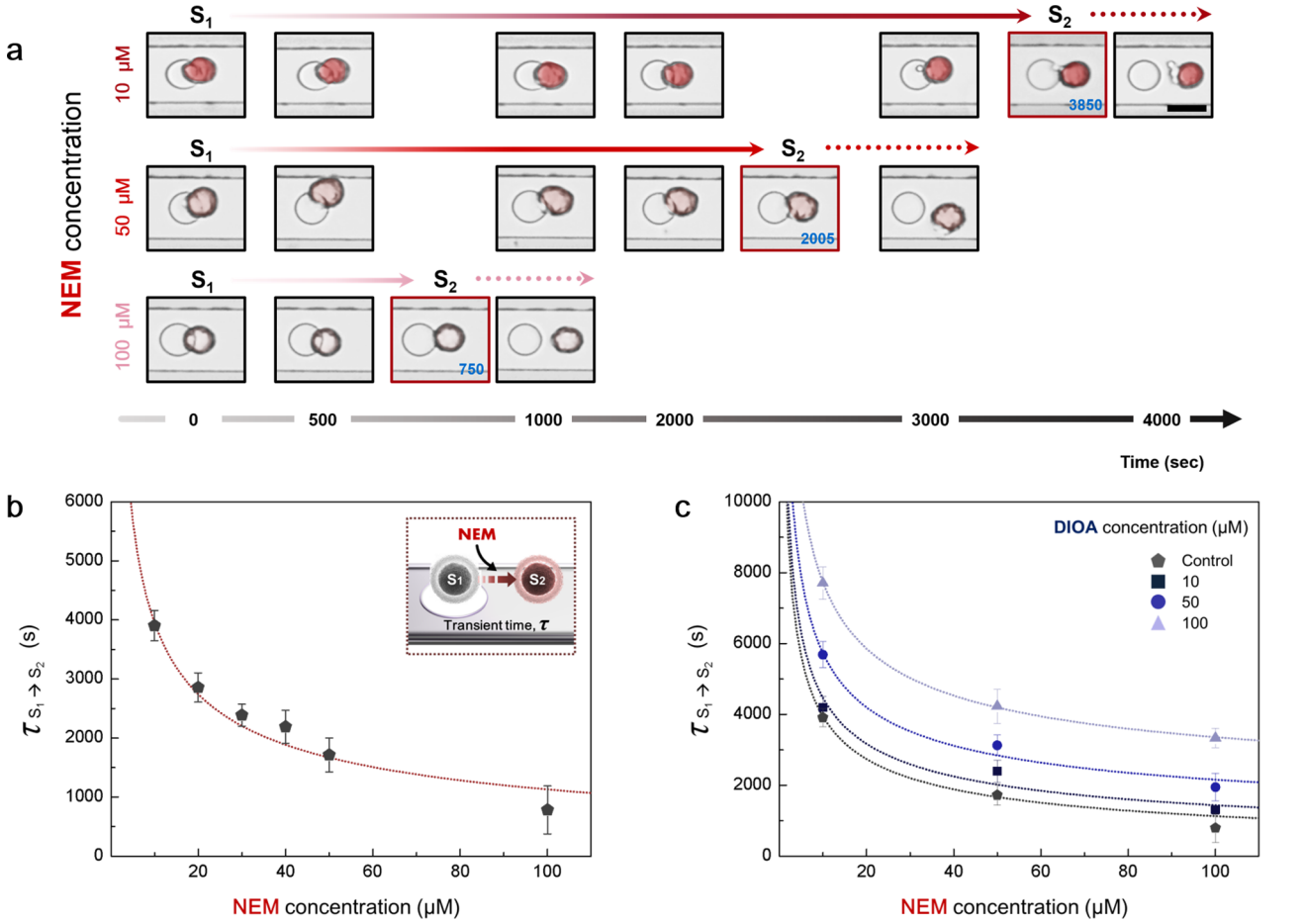

Figure 3. Cellular dynamics and cell activation in response to small-molecule drugs. (a) In situ monitoring of NEM-driven cell movement in which the cells were released from the trap window. The scale bar is 20 μm. (b) Transient time ($\tau_{S1\rightarrow S2}$) from a trapped state (i.e., normal cell; state 1) to a releasing state (i.e., NEM-treated cell; state 2) vs NEM concentration in μF-DEP-on-chip. (c) Transient time ($\tau_{S1\rightarrow S2}$) vs NEM concentration in the presence of another small-molecule drug, DIOA, which causes deactivation of KCC channels. Each data point represents at least 300 cell measurements.

observed. In addition, the behavior of dead cells when subjected to DEP forces clearly differs from that of live cells.[22] Therefore, it should be noted that the DEP manipulation of live B16F10 cells in our experimental conditions and after introducing drugs (NEM, DIOA, and NEM + DIOA) was not affected by toxicity or apoptosis. In addition, a previous report revealed that undesirable effects, such as Joule heating and electroporation through the cell membrane during DEP manipulation, were negligible at ac electric fields less than ~8 $V_{p\text{-}p}$ at low-frequency ranges (1−100 kHz) and in low-conductivity medium.[23] Therefore, for the entire experiment we set the electric field at 3 $V_{p\text{-}p}$ in the frequency range of 1−20 kHz to avoid any undesirable effects. Thus, the status of the ion channel in the cell membrane controlled by the addition of NEM and/or DIOA was the sole source of DEP manipulation. The upper panel of Figure 2b shows that individual cells in a buffer solution in the absence of any small-molecule drug were trapped around circular trap windows at 20 kHz. This was due to the positive DEP force acting on each cell that caused it to migrate toward the trap window. At 1 kHz, in contrast, individual cells moved away from the window and remained in the gap between the windows as a result of the negative DEP. Simulation results using dielectrophoretic theory, as shown in the bottom panel of Figure 2b, illustrate the DEP force vectors determining the movements of individual cells (a more detailed explanation of the numerical analysis is described in the Materials and Methods section and Supporting Information Note 1). Thus, through the comparison of both sets of results, we see that DEP forces acting on individual cells are positive at 20 kHz and negative at 1 kHz. After exposing the cell to different concentrations of NEM (10−100 μM) for 90 min, the DEP behavior of each cell was observed in the frequency range of 0−16 kHz. Figure 2c illustrates the experimental results for the number of cells that moved from the inside to the outside of a window at a certain frequency within the sweeping range after exposure to NEM. This figure shows that the frequencies at which DEP polarity (positive or negative) changes, called the crossover frequencies, were more widely distributed as NEM concentration increased. Since the data in Figure 2c can be fitted to a Gaussian distribution, the average crossover frequencies (± standard deviations) are 2.99 ± 0.01, 3.52 ± 0.04, 4.80 ± 0.06, and 6.92 ± 0.15 kHz in the absence of NEM (control) and with 10, 50, and 100 μM NEM, respectively. The coefficients of determination (R^2) of the average frequencies were 0.99, 0.98, 0.96, and 0.93 as the NEM concentration increased from 0 to 100 μM.

Dynamic Responses Caused by Variation in NEM and DIOA Concentrations. For a more comprehensive study of the drug effect on the cells we investigated the detailed processes induced by small-molecule drugs in individual

DOI: 10.1021/ac5041549
Anal. Chem. 2015, 87, 5914−5920

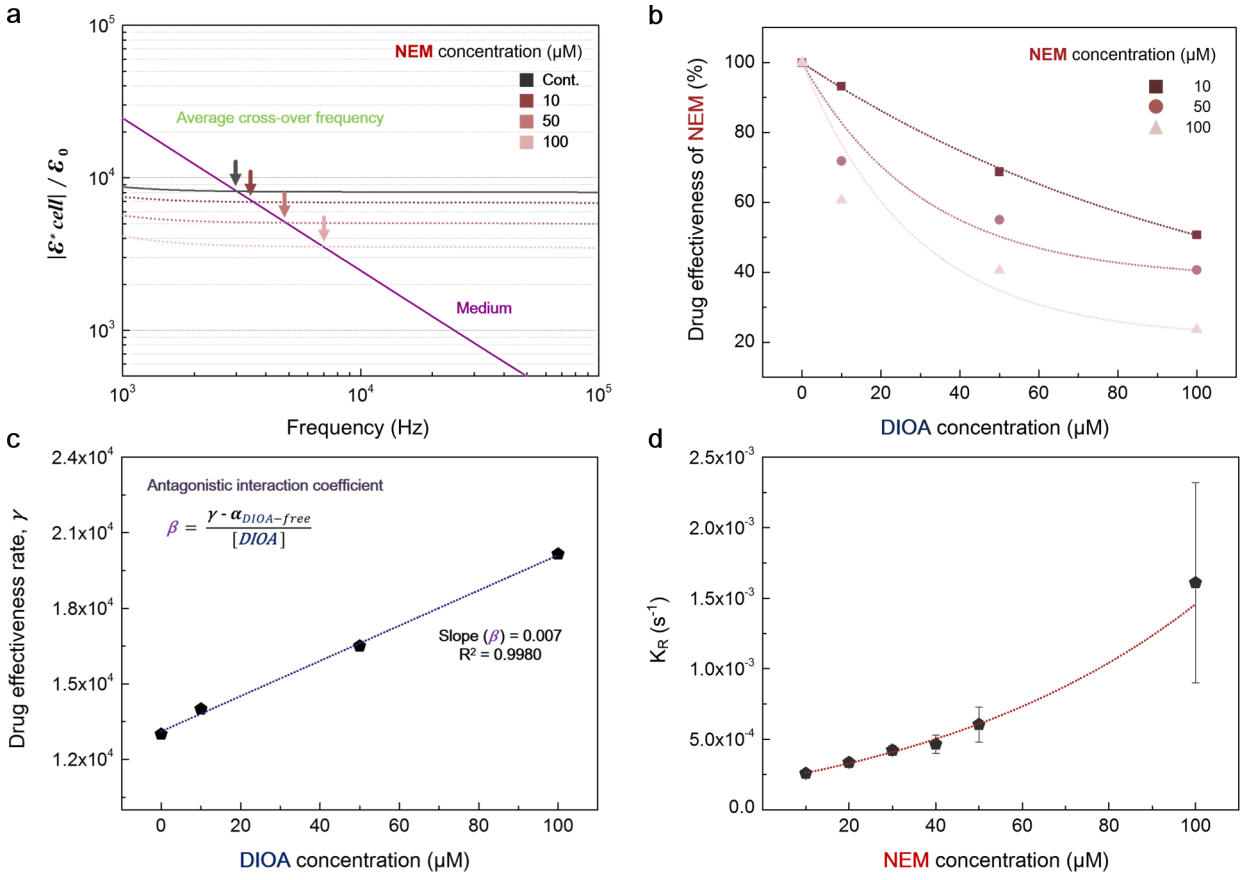

Figure 4. Quantitative numerical and experimental analysis of cellular static and dynamic responses to small-molecule drugs. (a) Calculated complex permittivities of the cell and medium as a function of frequency using the "single-shell" model in combination with measured crossover frequencies at different NEM concentrations. (b) NEM drug effectiveness (%) vs DIOA concentration indicating antagonistic interactions between NEM and DIOA in the cells; 100% of drug effectiveness of NEM describes the reference when no DIOA is applied. (c) Drug effectiveness rate (γ) vs DIOA concentration. (d) Kinetic rate ($k_R = 1/\tau_{s1\rightarrow s2}$) plotted vs NEM concentration.

B16F10 cells in terms of DEP capture. As a control, we showed that in the absence of NEM the cells were trapped around the trap window for a few hours at 3 kHz. In contrast, NEM-treated cells were released from the trap window at the same frequency. This observation indicates that the addition of NEM induces the reversal of DEP from positive to negative at a frequency of 3 kHz. Figure 3a shows time-lapse optical images of the movement of individual live cells away from a trap window at different concentrations of NEM. To explain the results of the present experiment, we define the transient time, $\tau_{s1\rightarrow s2}$, that represents the time required for the cell to migrate from state 1 (S_1) to state 2 (S_2), where S_1 is the state of the cell trapped at the edge and S_2 is the state of the cell released from the trap window having a constant release rate (a more detailed description of transient time is included in Supporting Information Note 2). This defined transient time is thought to be a good measure for deciphering how fast cells respond to a given drug and was therefore used to investigate the dynamic response of the living cells exposed to the small-molecule drugs NEM and DIOA. Figure 3b shows that the transient time ($\tau_{s1\rightarrow s2}$) drastically decreased as a function of NEM concentration, or in other words, B16F10 cells responded faster to higher concentrations of NEM. The data were also a good fit with our model, $\tau_{s1\rightarrow s2} = \alpha[\mathrm{NEM}]^{-1/2}$. Here, α is defined as a drug effectiveness coefficient (1.3×10^4) that implies the KCC ion channel activation effect of a drug (in this case NEM) on a cell (in this case a B16F10 cell), which may play a critical role in the determination of drug effectiveness at the cellular level.[24] Next, using the transient time, we examined the antagonistic interaction between NEM and DIOA with respect to B16F10 cellular dynamic responses. As a deactivating chemical agent for the KCC channel, DIOA played a crucial role in decreasing the transient time, $\tau_{s1\rightarrow s2}$, resulting from the action of NEM on the cells (Figure 3c and Supporting Information Table S2). We also showed that DIOA was more effective in competitive reactions at higher concentrations of NEM. This defined transient time is thought to be a good measure for deciphering how fast cells respond to a given drug and was therefore used to investigate the dynamic response of the living cells exposed to the small-molecule drugs NEM and DIOA. Figure 3b shows that the transient time ($\tau_{s1\rightarrow s2}$) drastically decreased as a function of NEM concentration or, in other words, B16F10 cells responded faster to higher concentrations of NEM. The data were also a good fit with our model, $\tau_{s1\rightarrow s2} = \alpha[\mathrm{NEM}]^{-1/2}$. Here, α is defined as a drug effectiveness coefficient (1.3×10^4) that implies the KCC ion channel activation effect of a drug (in this case NEM) on a cell (in this case a B16F10 cell), which may play a critical role in the determination of drug effectiveness at the cellular level.[24] Next, using the transient time, we examined the antagonistic interaction between NEM and DIOA with respect to B16F10 cellular dynamic responses. As a deactivating chemical agent for the KCC channel, DIOA played a crucial role in decreasing the transient time, $\tau_{s1\rightarrow s2}$, resulting from the action of NEM on the

DOI: 10.1021/ac5041549
Anal. Chem. 2015, 87, 5914−5920

cells (Figure 3c and Supporting Information Table S2). We also showed that DIOA was more effective in competitive reactions at higher concentrations of NEM. To explain the results of the present experiment, we define the transient time, $\tau_{s1\rightarrow s2}$, that represents the time required for the cell to migrate from state 1 (S_1) to state 2 (S_2), where S_1 is the state of the cell trapped at the edge and S_2 is the state of the cell released from the trap window having a constant release rate (a more detailed description of transient time is included in Supporting Information Note 2). The transient time was increased by up to 350% at a NEM concentration of 100 μM and varying DIOA concentrations.

DISCUSSION

As described in the Results section, quantitative values regarding the static and dynamic cellular responses to NEM and DIOA were extracted using a novel label-free method that is related to the biological properties of a cell. To further understand the effects of small-molecule drugs on cellular response, we introduce several interesting parameters in this discussion. First, according to Figure 2c, the average crossover frequencies shifted from the lower region to the higher region with increasing NEM concentration. Using this phenomenon, the shiftiness of complex permittivity as a result of the introduced small drug can be extracted. The solid lines in Figure 4a show the theoretical complex permittivity ($|\varepsilon^*_{cell}|/\varepsilon_0$) of the cell and medium as a function of frequency in the absence of NEM (a detailed description of this calculation is provided in Supporting Information Note 1). There is also a point at which both complex permittivities are equivalent at a certain frequency (Figure 4a), which is the crossover frequency extracted from the theoretical model.[25] This calculated frequency exactly matched the experimental average crossover frequency shown in Figure 2c, in which the complex permittivity of the cell at this crossover frequency is 2.99 kHz. Moreover, the change in complex permittivity of the medium was negligible after NEM treatment of the cells because the solution volume was much larger than the small-molecule drug volume (Supporting Information Table S3). Accordingly, activation of KCC channels on the cell membrane does not change the ion composition or concentration of the cell exterior (medium), but does affect the cell interior, and a higher NEM concentration leads to faster ion release from the cell interior to the cell exterior. As a result, at the average crossover frequency was changed, as shown in Figure 2c. By associating the unchanged complex permittivity of the medium with the average crossover frequency variations, the complex permittivity of the cell could be shifted more and more by increasing NEM concentration, as shown in Figure 4a. Through monitoring this variation in complex permittivity of the cell with respect to NEM concentration, we can predict the electrical polarizability of a cell, which is changed by the degree of activation of KCC channels on the cell membrane.

Antagonistic interactions, which describe the effects of combinations of different small-molecule drugs on a cell, can also be quantitatively examined using our label-free and probeless measurement method. The normalized drug effectiveness caused by the antagonistic interaction in which NEM is the activator and DIOA is the specific inhibitor to reduce the NEM effect is shown in Figure 4b. The graph in Figure 4b shows that NEM effectiveness in B16F10 cells was mitigated in the presence of DIOA and was notably reduced by up to 20% with DIOA concentrations up to 100 μM. Furthermore, we also extracted the antagonistic interaction coefficient (β) that represents how the NEM activation rate of the KCC channels on the cell membrane is reduced with inhibition by DIOA. As shown in Figure 4c, β was found to be 0.007 with different DIOA concentrations of 0−100 μM, illustrating that the influence of the antagonistic interaction can be simply modeled as $\beta = (\gamma - \alpha_{DIOA\text{-}free})/[DIOA]$, where β is the antagonistic interaction coefficient, γ is the antagonistic interaction rate, and $\alpha_{DIOA\text{-}free}$ is the NEM effectiveness coefficient in the absence of DIOA that had already been determined in Figure 3b. Quantitative and statistical analysis of antagonistic interactions using this model is expected to be useful for predicting and evaluating multiple drug−cell interactions at the cellular level. Figure 4d represents the kinetic rate ($k_R = 1/\tau_{s1\rightarrow s2}$) as a function of NEM concentration. Since this kinetic rate corresponds to the number of ions within the B16F10 cell that are released to the outside of the cell with a change in NEM concentration, it can be used to evaluate the real-time drug influence on the B16F10 cells. According to Figure 4d, the kinetic rate of the live B16F10 cells affected by NEM is exponentially proportional to the NEM concentration in the cell medium.

Moreover, it is noteworthy that larger standard deviations in the kinetic rate of dynamic cellular responses were observed at higher NEM concentrations. This trend was also observed in the cellular static response, as shown in Figure 2c. In particular, the fwhm, which is the difference between two frequency values of the half-maximum value in the Gaussian distribution function, represents the width of the Gaussian distribution. As shown in Figure 2c, the fwhm's were 0.99, 1.44, 1.78, and 4.73 kHz at NEM concentrations of 0, 10, 50, and 100 μM, respectively. Hence, a high fwhm for the distribution and a large standard deviation measured at high NEM concentrations imply that the response of each cell exposed to NEM varied more as NEM concentration increased. In addition, previous reports have shown that the KCC channels play a significant role in maintaining the ionic and osmotic homeostasis of many cell types.[26,27] Therefore, the functional capability of the KCC channels in each of the B16F10 cells, which work equivalently in the absence of NEM to maintain homeostasis, would be subdivided by the different adaptability abilities of each cell when the NEM concentration is increased. The quantified fwhm or standard deviation of the kinetic rate is a useful indicator to investigate the diversity of the functional capability of KCC channels of individual cells with respect to the influence of small-molecule drugs such as NEM or DIOA. However, further investigation is needed to more clearly elucidate the diversity of functional capability in KCC channels of B16F10 cells.

In conclusion, we investigated static and dynamic cellular biological properties within a microfluidic dielectrophoresis device using a novel technique for analyzing cell biological properties after cellular exposure to NEM, DIOA, or their combination. In this study, experimental results for the variation in DEP properties that were attributed to changes in ion transport through the KCC channels on the cell membrane as a result of exposure to small-molecule drugs were quantitatively and statistically analyzed. In the static responses, the shift of the complex permittivity of B16F10 cells according to the drug concentration was reported for the first time using our DEP model and data analysis. Moreover, in the dynamic responses, the effect of the small-molecule drugs on the DEP behavior of the cells was observed in real time. According to

DOI: 10.1021/ac5041549
Anal. Chem. 2015, 87, 5914−5920

these observations, we defined transient time to provide a better understanding of the dynamic responses of the cell. On the basis of data for the measured transient time, we investigated the usefulness of parameters including the drug effectiveness coefficient, kinetic rate, antagonistic interaction coefficient, and fwhm to evaluate cellular responses to a drug. Among these parameters, the drug effectiveness coefficient and kinetic rate were good measurable quantities representing the real-time influence of drugs on the cell. Antagonistic interaction coefficients were good factors indicating the interactions of different types of drugs with cells and the effects on cell properties. The fwhm and standard deviation of kinetic rate were good indicators for examining the variation of ionic channel functional capability in individual cells with increasing concentration of a drug. Our results demonstrate that the technique of analyzing cell biological properties within a microfluidic dielectrophoresis device can serve as a powerful tool for examining 3D cellular responses to small-molecule drugs, thereby providing useful information on the cellular biological properties affected by small-molecule drugs at the single-cell level.

■ ASSOCIATED CONTENT

Supporting Information

Details on experimental result, fabrication process, and numerical analysis of the dielectrophoretic force acting on B16F10 cells and cellular transient time. This material is available free of charge via the Internet at http://pubs.acs.org.

■ AUTHOR INFORMATION

Corresponding Author

*Phone: +82-33-760-2791. E-mail: yusuklee@yonsei.ac.kr.

Author Contributions

I.S.P. and J.L. contributed equally to this work.

Notes

The authors declare no competing financial interest.

■ ACKNOWLEDGMENTS

This research was supported by grants from the National Research Foundation (NRF) funded by the Ministry of Education, Science, and Technology (NRF-2013R1A2A2A03005767), Republic of Korea.

■ REFERENCES

(1) Cross, S. E.; Jin, Y. S.; Rao, J.; Gimzewski, J. K. *Nat. Nanotechnol.* **2007**, *2*, 780−783 DOI: 10.1038/nnano.2007.388.

(2) Rotsch, C.; Radmacher, M. *Biophys. J.* **2000**, *78*, 520−535 DOI: 10.1016/S0006-3495(00)76614-8.

(3) Park, G. S.; Kwon, H.; Kwak, D. W.; Park, S. Y.; Kim, M.; Lee, J. H.; Han, H.; Heo, S.; Li, X. S.; Lee, J. H.; Kim, Y. H.; Lee, J. G.; Yang, W.; Cho, H. Y.; Kim, S. K.; Kim, K. *Nano Lett.* **2012**, *12*, 1638−1642 DOI: 10.1021/nl2045759.

(4) Cohen-Karni, T.; Qing, Q.; Li, Q.; Fang, Y.; Lieber, C. M. *Nano Lett.* **2010**, *10*, 1098−1102 DOI: 10.1021/nl1002608.

(5) Xie, C.; Lin, Z.; Hanson, L.; Cui, Y.; Cui, B. *Nat. Nanotechnol.* **2012**, *7*, 185−190 DOI: 10.1038/nnano.2012.8.

(6) Tian, B.; Cohen-Karni, T.; Qing, Q.; Duan, X.; Xie, P.; Lieber, C. M. *Science* **2010**, *329*, 830−834 DOI: 10.1126/science.1192033.

(7) Duan, X.; Gao, R.; Xie, P.; Cohen-Karni, T.; Qing, Q.; Choe, H. S.; Tian, B.; Jiang, X.; Lieber, C. M. *Nat. Nanotechnol.* **2011**, *7*, 174−179 DOI: 10.1038/nnano.2011.223.

(8) Gao, R.; Strehle, S.; Tian, B.; Cohen-Karni, T.; Xie, P.; Duan, X.; Qing, Q.; Lieber, C. M. *Nano Lett.* **2012**, *12*, 3329−3333 DOI: 10.1021/nl301623p.

(9) Wang, X. B.; Yang, J.; Huang, Y.; Vykoukal, J.; Becker, F. F.; Gascoyne, P. R. C. *Anal. Chem.* **2000**, *72*, 832−839 DOI: 10.1021/ac990922o.

(10) Shafiee, H.; Sano, M. B.; Henslee, E. A.; Caldwell, J. L.; Davalos, R. V. *Lab Chip* **2010**, *10*, 438−445 DOI: 10.1039/b920590j.

(11) Ratanachoo, K.; Gascoyne, P. R.; Ruchirawat, M. *Biochim. Biophys. Acta, Biomembr.* **2002**, *1564*, 449−458 DOI: 10.1016/S0005-2736(02)00494-7.

(12) Hsiung, L. C.; Chiang, C. L.; Wang, C. H.; Huang, Y. H.; Kuo, C. T.; Cheng, J. Y.; Lin, C. H.; Wu, V.; Chou, H. Y.; Jong, D. S.; Lee, H.; Wo, A. M. *Lab Chip* **2011**, *11*, 2333−2342 DOI: 10.1039/c1lc20147f.

(13) Kang, Y.; Li, D.; Kalams, S. A.; Eid, J. E. *Biomed. Microdevices* **2008**, *10*, 243−249 DOI: 10.1007/s10544-007-9130-y.

(14) Lapizco-Encinas, B. H.; Simmons, B. A.; Cummings, E. B.; Fintschenko, Y. *Anal. Chem.* **2004**, *76*, 1571−1579 DOI: 10.1021/ac034804j.

(15) Lee, S. W.; Li, H.; Bashir, R. *Appl. Phys. Lett.* **2007**, *90*, 223902 DOI: 10.1063/1.2744483.

(16) Baek, S. H.; Chang, W. J.; Baek, J. Y.; Yoon, D. S.; Bashir, R.; Lee, S. W. *Anal. Chem.* **2009**, *81*, 7737−7742 DOI: 10.1021/ac901211b.

(17) Park, I. S.; Eom, K.; Son, J.; Chang, W. J.; Park, K.; Kwon, T.; Yoon, D. S.; Bashir, R.; Lee, S. W. *ACS Nano* **2012**, *104*, 8665−8673 DOI: 10.1021/nn302202t.

(18) Valente, P.; Fassina, G.; Melchiori, A.; Masiello, L.; Cilli, M.; Vacca, A.; Onisto, M.; Santi, L.; Stetler-Stevenson, W. G.; Albini, A. *Int. J. Cancer* **1998**, *75*, 246−253 DOI: 10.1002/(SICI)1097-0215(19980119)75:2<246::AID-IJC13>3.0.CO;2-B.

(19) Yoon, N. Y.; Eom, T. K.; Kim, M. M.; Kim, S. K. *J. Agric. Food Chem.* **2009**, *57*, 4124−4129 DOI: 10.1021/jf900006f.

(20) Shen, M. R.; et al. *Proc. Natl. Acad. Sci. U.S.A.* **2001**, *98* (25), 14714−14719 DOI: 10.1073/pnas.251388798.

(21) Vitoux, D.; Olivieri, O.; Garay, R. P.; Cragoe, E. J.; Galacteros, F.; Beuzard, Y. *Proc. Natl. Acad. Sci. U.S.A* **1989**, *86*, 4273−4276.

(22) Park, I. S.; Park, S. H.; Lee, S. W.; Dae, S. Y.; Kim, B.-M. *Appl. Phys. Lett.* **2014**, *104*, 053701 DOI: 10.1063/1.4862746.

(23) Huang, C.; Liu, C.; Loo, J.; Stakenborg, T.; Lagae, L. *Appl. Phys. Lett.* **2014**, *104*, 013703 DOI: 10.1063/1.4861135.

(24) Sharma, S. V.; Lee, D. Y.; Li, B.; Quinlan, M. P.; Takahashi, F.; Maheswaran, S.; McDermott, U.; Azizian, N.; Zou, L.; Fischbach, M.; Wong, K. K.; Brandstetter, K.; Wittner, B.; Ramaswamy, S.; Classon, M.; Settleman, J. *Cell* **2010**, *141*, 69−80 DOI: 10.1016/j.cell.2010.02.027.

(25) Valero, A.; Braschler, T.; Renaud, P. *Lab Chip* **2010**, *10*, 2216−2225 DOI: 10.1039/C003982A.

(26) Klein, T.; Cooper, T. G.; Yeung, C. H. *Biol. Reprod.* **2006**, *75*, 853−858 DOI: 10.1095/biolreprod.106.054064.

(27) Shen, M. R.; Chou, C. Y.; Hsu, K. F.; Hsu, Y. M.; Chiu, W. T.; Tang, M. J.; Alper, S. L.; Ellory, J. C. *J. Biol. Chem.* **2003**, *278*, 39941−39950 DOI: 10.1074/jbc.M308232200.

(28) Sabuncu, A. C.; Liu, J. A.; Beebe, S. J.; Beskok, A. *Biomicrofluidics* **2010**, *4*, 021101 DOI: 10.1063/1.3447702.

(29) Morgan, H.; Green, N. G. *AC Electrokinetics: Colloids and Nanoparticles*; Research Studies Press: Baldock, U.K., 2003; pp 33−47.

(30) Wang, X.; Ha, T. *Science* **2013**, *340*, 991−994 DOI: 10.1126/science.1231041.

DOI: 10.1021/ac5041549
Anal. Chem. 2015, 87, 5914−5920